J. Fluid Mech. (1970), *vol.* 41, *part* 3, *pp.* 655–672
Printed in Great Britain

Gravity wave refraction by islands

By CONRAD C. LAUTENBACHER
Harvard University, Cambridge, Massachusetts

(Received 23 January 1969 and in revised form 27 August 1969)

The refractive influence on tsunami run-up of the offshore bottom topography of islands is analyzed. Shallow water theory is used to treat problems in which the geometry resembles that of individual Hawaiian islands and in which the incident wave is plane and monochromatic.

Mathematically, the differential equation for long-wave propagation is converted into an integral equation to which numerical methods are applied. Results of practical importance include the run-up on island coastal areas. The results are used in conjunction with earlier one-dimensional analyses to estimate the total tsunami run-up.

1. Introduction

Tsunamis (or seismic sea waves) are long wave trains on the surface of the oceans generated by earthquakes, volcanoes, fault movements, or other general dislocations occurring on land surfaces contiguous with or contained within the oceans. The majority of the energy carried by a seismic sea wave is concentrated in the section of ocean wavelength spectrum between thirty and four-hundred miles. Wave amplitudes on the open ocean are of the order of one foot, while coastal amplitudes may be as high as 30 or 40 ft.

A reasonably general theory of one-dimensional tsunami run-up is given in a paper by Carrier (1966). There, the run-up of a tsunami initiated by a distant ocean bottom disturbance, propagated over an irregular bottom, and amplified by a sloping beach is analyzed. The maximum wave run-ups calculated are smaller than those on islands, and one could conjecture that the discrepancy is due to absence, in the theory, of the effect of refractive focusing. The following study supports this hypothesis.

2. Formulation of the problem

Long wavelengths and small amplitudes imply that linear long wave theory is appropriate. Nonlinear effects are present in a small region adjacent to a coast and will be discussed further in § 5.

In such a theory,

$$(h''\eta'_{\bar{x}})_{\bar{x}} + (h''\eta'_{\bar{z}})_{\bar{z}} - \frac{1}{g}\eta'_{tt} = 0, \tag{1}$$

where g is acceleration of gravity, h'' is water depth, η' is wave height (above undisturbed water level), $\bar{x}, \bar{z}$ are horizontal Cartesian co-ordinates and t is time (letter subscripts indicate differentiation).

Solutions for (1) will be determined in regions whose topographies are idealizations of island topographies, e.g. the frustums of circular and elliptical cones. Figure 1 depicts island geometry and lists data for the circular islands and wavelengths investigated. The results depend on two non-dimensional parameters, L/R (see figure 1), and λ/L, the ratio of wavelength to island base diameter. The relation between the wavelength and the period of the incident wave also depends on the water depth at the island base. Solutions obtained thus apply to all islands with non-dimensional parameters identical to the cases investigated.

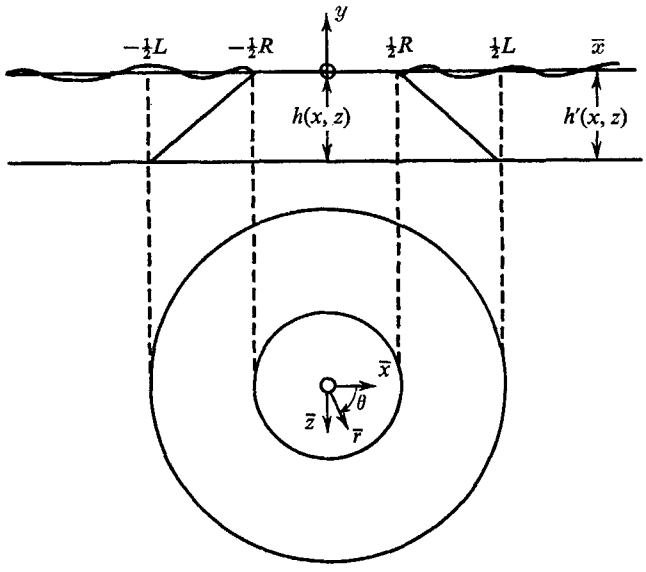

FIGURE 1. Islands investigated. $r = (\bar{x}^2+\bar{z}^2)^{\frac{1}{2}}$; h_0 = dimensional water depth in $\bar{r} > \frac{1}{2}L$. nm, nautical mile; λ, wavelength; T, period.

L/R	Model	L (nm)	h_0 (fm)	λ/L	T (min)
4·65	Small	50	3000	0·785, 3·35, 7·85	5, 22, 50
4·00	Oahu	100	2500	1, 2, 4	14, 28, 57
1·67	Hawaii	125	3000	1, 2, 4	17, 34, 69

It is of particular interest to infer tsunami run-up on island shores. In pursuit of this goal, the solution for a particular frequency ω will be obtained for incident waves of the form,

$$\eta_i' = \eta_0 \exp\{i(k'\bar{x} - \omega t)\}.$$

The following non-dimensional variables are used for ease in calculation and interpretation:

$$\eta(x, z)\, e^{-i\omega t} = \frac{\eta'}{\eta_0}; \quad h' = \frac{h''}{h_0}; \quad x = \frac{\bar{x}}{L}; \quad z = \frac{\bar{z}}{L}; \quad k = k'L.$$

$k' = \left(\frac{\omega^2}{gh_0}\right)^{\frac{1}{2}}$, η_0 is the incident wave amplitude, and h_0 is indicated in figure 1.

In terms of the new variables, the long-wave equation becomes

$$(h'\eta_x)_x + (h'\eta_z)_z + k^2\eta = 0. \tag{2}$$

The following comments anticipate the use of numerical methods. The differential long-wave equation is elliptic in nature over an infinite region. Thus, the direct calculation of a numerical solution is extremely inconvenient. As is well-known, a solution to the differential equation exists and is unique in a region, provided that suitable conditions are prescribed on every section of the boundary of the region. In a closed domain with known boundary conditions, an elliptic equation is solved numerically by replacing the differential operators with finite difference operators. The result is a set of algebraic equations for the function values at discrete points of the region. Solution accuracy is checked by increasing the number of points in the region and comparing results.

The problem of wave scattering by an island involves an open region. Obviously, a finite difference solution of the differential equation requires termination of the open region at some finite value. To be assured of a correct numerical solution, the wave form must be known at the assumed outer boundary. The only restriction is that the solution obey the radiation condition, i.e. scattered wave energy must propagate away from the island. In a constant depth region, the solution may be expressed as an infinite Fourier–Bessel series with indeterminate coefficients. Choosing Hankel functions for outgoing waves satisfies the radiation condition. However, the precise form of the wave at any radius cannot be known, *a priori*.

As a first approximation, the Hankel functions in the expansion of the far field may be replaced by their asymptotic forms. Such an approach was used by Vastano & Reid (1967) to investigate numerical long-wave solutions in the neighbourhood of a circular cylinder on a constant-depth bottom, and in the region of a paraboloid bounded by a shore line wall at a depth 10 % of the island base depth. Results for each set of parameters must be checked carefully to validate the choice of outer boundary position and the use of the asymptotic form of the radiation condition.

Vastano & Reid (1966) extended their computations to include conical islands together with a model retaining some of the real topographical features of Wake Island, all with a coast line wall. None of the cases solved by Vastano & Reid were sufficiently similar to those investigated in this paper to allow a direct quantitative comparison, but solution curves of similar character from both papers are pictured in figure 2 for reference.

In the method of Vastano & Reid, the only possible coastal boundary condition is that of no-flow. Any island investigated is automatically surrounded by a wall. The treatment developed below has no such limitation but includes the proper boundary condition on a sloping beach with no wall. An interesting observation is that the method of this paper could not cover a no-flow condition at the coast, while the method of Vastano & Reid includes no-flow at the coast as the only possible condition.

For long (non-breaking) waves of small amplitude, no viscous energy dissipation of significant proportions occurs on a sloping beach. This condition may be approximated in the solution of (non-viscous) long-wave theory by enforcing no energy absorption at the coast. The one-dimensional, linear, bounded solution on a beach of constant slope (see § 4) allows no energy absorption or creation.

The only tractable one-dimensional, nonlinear solution, which models details of the coastal flow exactly, also results in no energy absorption at the coast. (See Carrier & Greenspan 1958.)

Furthermore, the nonlinear solution away from the coast becomes precisely that of the linear theory requiring a bounded solution at the undisturbed shore line. The derivation of the longwave integral equation (§ 2) makes no quantitative demands on the value of the wave height or its derivatives at the coast. A bounded solution at the coast is enforced implicitly in the numerical method. One-dimensional results were checked, verifying that the analytic solution of the differential equation exactly matched that obtained numerically from the integral equation.

3. Formulation of the integral equation

The technique developed below for solving the long-wave equation automatically includes the precise radiation condition. Specifically, the differential equation is converted into a finite range integral equation. Dependence of numerical calculations upon the choice of region and approximate radiation condition is eliminated.

The wave height is described by

$$\eta = e^{ik(x+\frac{1}{2})} + w(x,z).\dagger$$

The first term is the incident monochromatic wave and is an exact solution of (2) in a domain excluding the island. The second term represents the wave scattered from the island. The depth is measured from the ocean floor, and, in the new coordinate system, has the value unity at the undisturbed water level,

$$h = 1 - h'.$$

By substituting the new variables and utilizing the outgoing wave Green's function for the Helmholtz equation in an infinite region, i.e. $i\pi H_0^{(1)}(kR_1)$, an integral equation is derived (see appendix A):

$$(1-h)\,w(x,z) = -\frac{i}{4}\iint\left\{-k^2 H_0^{(1)}(kR_1)\,h + kH_1^{(1)}(kR_1)\left[\frac{x-x'}{R_1}h_{x'} + \frac{z-z'}{R_1}h_{z'}\right]\right\}$$

$$\times\, w(x',z')\,dx'\,dz' + \frac{1}{4}\iint kH_0^{(1)}(kR_1)\,e^{ik(x'+\frac{1}{2})}(h_{x'} + ikh)\,dx'\,dz', \quad (3)$$

where $R_1 = ((x-x')^2 + (z-z')^2)^{\frac{1}{2}}$. The range of integration includes only the submerged parts of the island.

† The factor $e^{\frac{1}{2}ik}$ is included in the incident wave representation for algebraic convenience in solving for the analytic, one-dimensional solution of the scattered wave $w(x)$. The factor remains in the two-dimensional incident wave representation for comparing the numerical solutions $w(x)$ and $w(x, z)$ with the analytic $w(x)$.

4. Method of solution

Equation (3) was solved numerically with the aid of an IBM 7094 computer. For circular islands, polar co-ordinates and circular grids were employed. The unknown was determined at intersections of the grid lines with quadrature formulae developed by assuming a biquadratic polynomial form over every mesh division of nine points. Quadrature coefficients were calculated by integrating over the block of the dual grid centred on the middle of the nine points under consideration. In this manner, a set of complex, linear, algebraic equations was developed for the values of the unknown at each grid point.

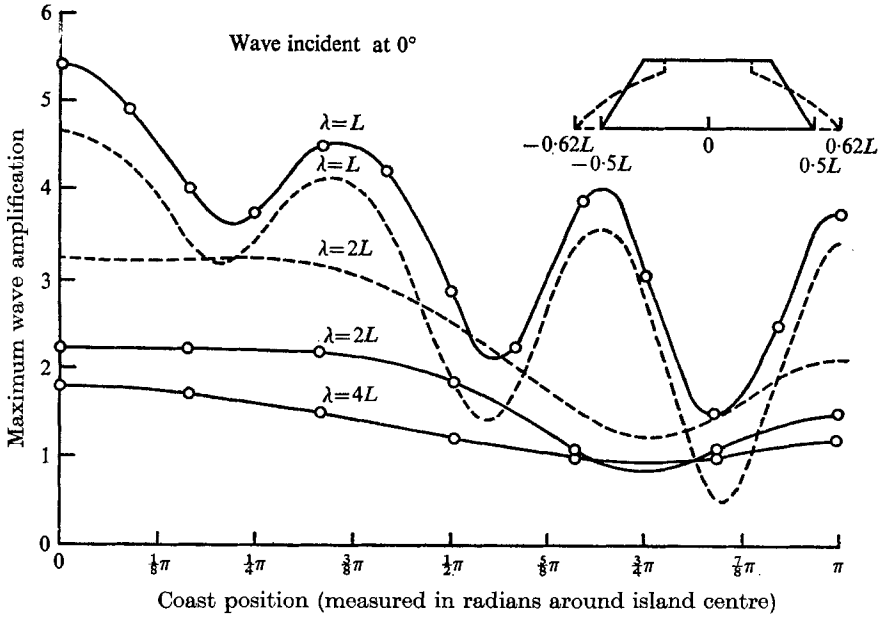

FIGURE 2. Maximum wave amplification at coast (Hawaii).
– – –, Vastano & Reid (1966, p. 227).

This set of equations was solved for varying island size, slope, height and wavelength. Solutions for elliptical islands were obtained by transforming the equation to elliptical co-ordinates and employing an elliptical mesh. The ensuing pages illustrate various interesting solution characteristics. Numerical details are presented in appendix B.

Figures 2–4 are plots of the maximum wave amplitude at the coast around a half-island. The island–wave system is symmetrical with respect to a line through the island centre perpendicular to the incoming wave fronts at infinity.

Figure 5 depicts the maximum wave amplitude around the coast of an elliptical island whose major axis is twice the minor axis. The incoming wave fronts are perpendicular to the major axis. For comparison with the circular islands, the elliptical island cross-section along the minor axis is identical with that of the 'small' island, as shown in figure 1. Due to the nature of elliptical co-ordinates, the island base is practically circular. The position at the coast in figure 5 is

measured in terms of the elliptical angular co-ordinate ϕ. Figure 6 depicts the maximum wave amplitude around the coast of an identical elliptical island except that the minor axis is perpendicular to the incoming wavefronts.

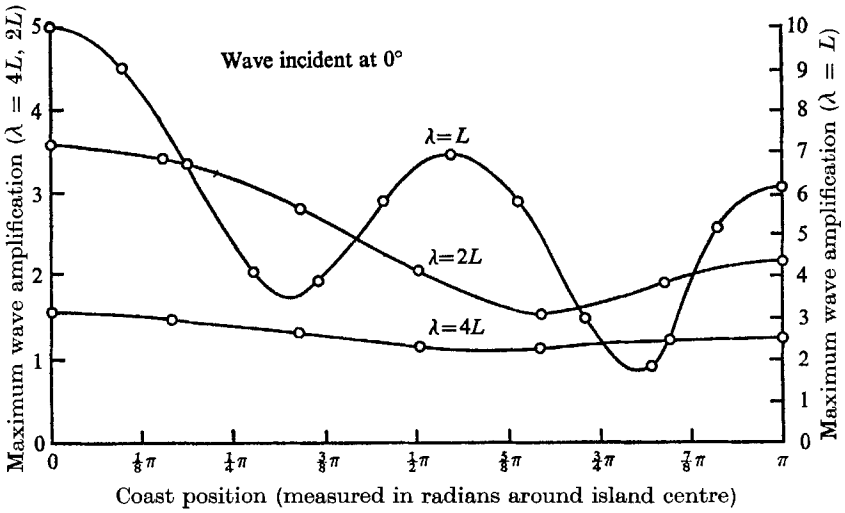

FIGURE 3. Maximum wave amplification at coast (Oahu).

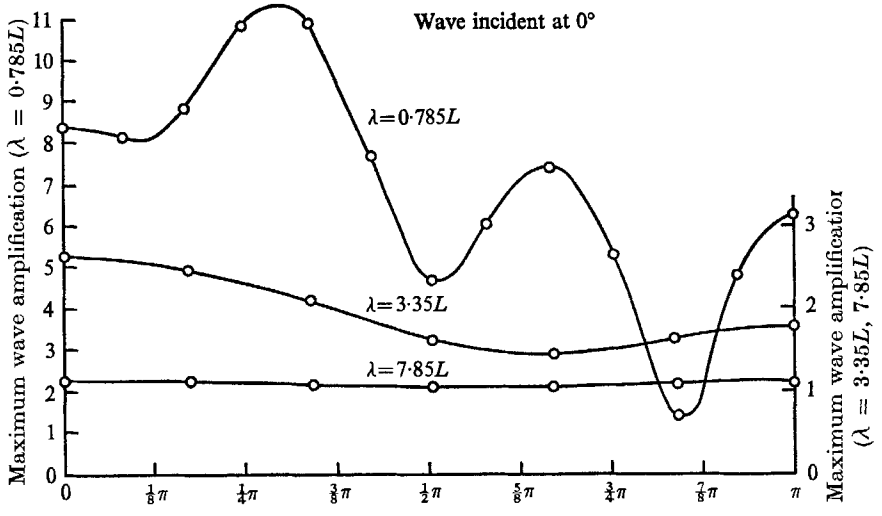

FIGURE 4. Maximum wave amplification at coast.

Figure 2 contains the best possible match of solutions from the present study and from the work of Vastano & Reid. After matching results, the island shapes necessary to obtain these curves in each study were compared. As noted in figure 2, the island shapes differ, a result of dissimilar coastal boundary configurations. The present study contains islands of constant slope over the entire distance between shore line and island base. The coastal wall used by Vastano &

Reid acts to reduce considerably the maximum wave height. Eliminating the section of sloping beach nearest the shore line removes a major portion of the wave focusing mechanism.

An appreciation of amplification differences caused by coastal configurations may be gained by recognizing that an island shape comparable to that of Vastano

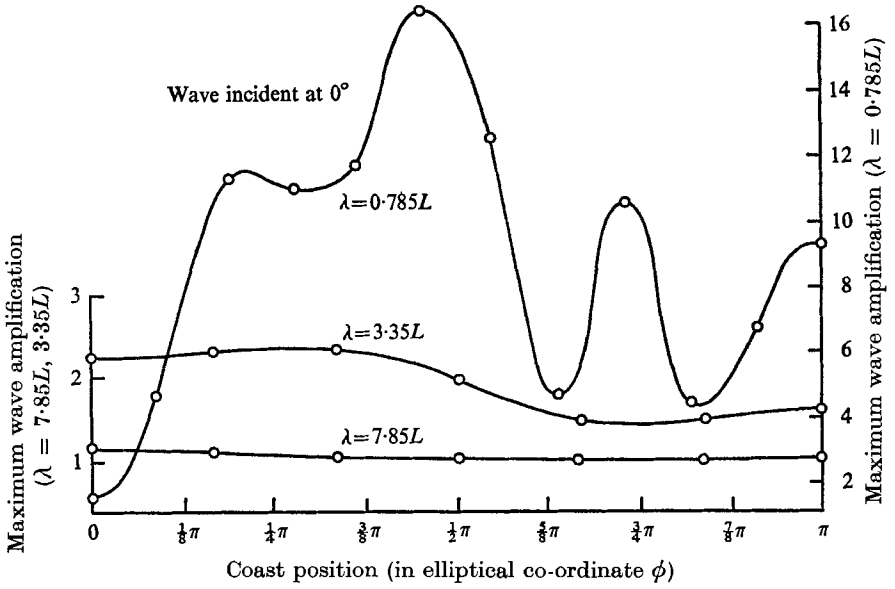

FIGURE 5. Maximum wave amplification at coast (elliptical island, major axis perpendicular to wavefronts).

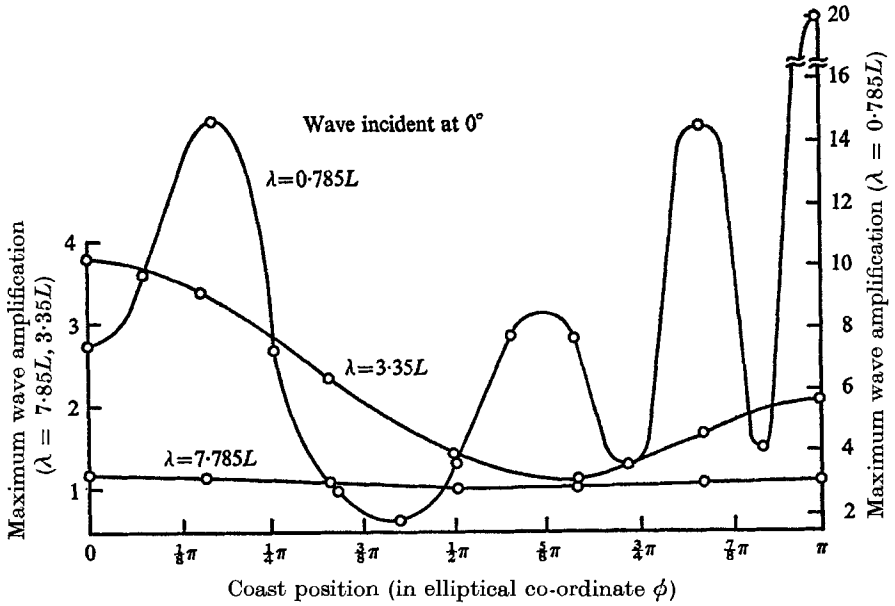

FIGURE 6. Maximum wave amplification at coast (elliptical island, minor axis perpendicular to wavefronts).

& Reid in figure 2 yields much greater amplitudes in the present study. Figure 3 is such a sample, and, for the shortest wavelength, depicts a maximum amplitude almost twice that of Vastano & Reid in figure 2. Furthermore, the number of peaks in the coastal amplification curves decreases from four in figure 2 to three in figure 3.

5. One-dimensional wave theory

(i) *Linear long wave theory*

For comparison with the two-dimensional long-wave solutions, the analytic results of the one-dimensional linear theory are developed below (see figure 7).

With only one horizontal co-ordinate, the island reduces to an infinite ridge running perpendicular to the plane of the paper. Regions 1 and 2 have no physical

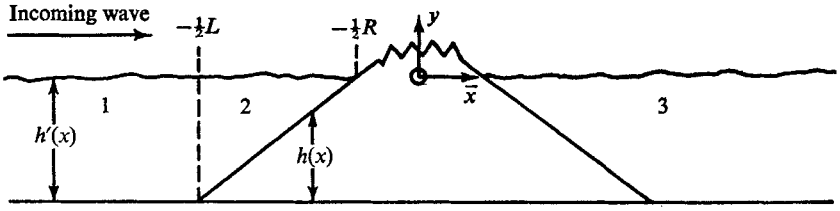

FIGURE 7. One-dimensional island geometry.

connection with region 3 and the solution is limited solely to regions 1 and 2. The ridge is subjected to a monochromatic wave propagating to the right from $x = -\infty$. With the assumption $\eta(x,t) = \eta(x)\, e^{-i\omega t}$, the equation becomes

$$(h'\eta_x)_x + k^2\eta = 0. \tag{4}$$

The non-dimensional variables are identical to those used previously, with the exception that z is no longer present. The problem as posed is completely analagous to the two-dimensional formulation.

The depth in region 1 is $h' = 1$; and, in region 2, $h' = \alpha x + d$. The solutions are

$$(1) \quad \eta = e^{ik(x+\frac{1}{2})} + B\, e^{-ik(x+\frac{1}{2})},$$

$$(2) \quad \eta = CJ_0\left(\frac{2k\sqrt{h'}}{|\alpha|}\right).$$

(J_0 and J_1 are Bessel functions of the first kind.) In region 2, the selection of the bounded solution is consistent with the energy argument presented in § 1. C and B are determined by matching wave height and slope at the boundary of 1 and 2:

$$C = \frac{2}{J_0\left(\frac{2k}{|\alpha|}\right) + iJ_1\left(\frac{2k}{|\alpha|}\right)}, \quad B = \frac{J_0\left(\frac{2k}{|\alpha|}\right) + iJ_1\left(\frac{2k}{|\alpha|}\right)}{J_0\left(\frac{2k}{|\alpha|}\right) - iJ_1\left(\frac{2k}{|\alpha|}\right)}.$$

The matching conditions ensure the continuity of wave height and particle velocity at $x = -\frac{1}{2}$.

In figure 8, several representative solutions are compared with their two-dimensional counterparts. Note that the two-dimensional maximum amplification does not surpass one-dimensional maximum amplification until $\lambda < 2L$.

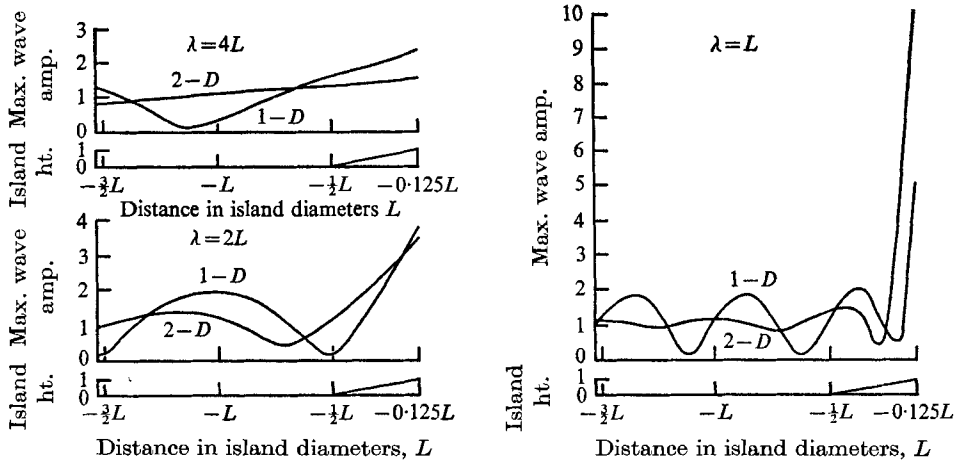

FIGURE 8. Comparison of one-dimensional and two-dimensional maximum wave amplitudes on line of reflective symmetry (Oahu).

(ii) *Nonlinear wave theory*

Pertinent to the commentary in § 5 is Carrier's (1966) expression for the wave amplification on a one-dimensional sloping beach. Briefly, Carrier solves an initial value problem with deep-water dispersive wave theory in a region of constant depth from tsunami source to the base of the sloping beach. The purpose of this calculation is the determination of an appropriate tsunami spectrum at the island base to serve as a condition to the solution of the nonlinear shallow water equations on the sloping beach (Carrier & Greenspan 1958).

The result of the analysis is a beach amplification factor, the ratio of the maximum wave height at the coast and the maximum wave height at the base of the sloping beach.

$$A = \eta(\text{coast})_{\max}/\eta(\text{base})_{\max}.$$

The maximum wave heights are evaluated from integrals by the method of stationary phase. The point of stationary phase is a particular wave-number in a complex wave-number plane, implying that the maximum amplification is due to the contributions of a narrow band centred on the point of stationary phase.

The results are:

$$\text{maximum run-up wave-number} \sim x_0^{-\frac{1}{3}},$$

$$A = \begin{cases} 4{\cdot}2\beta^{-\frac{1}{2}}x_0^{-\frac{1}{8}}, & \text{initial motion upward,} \\ 5{\cdot}6\beta^{-\frac{1}{2}}x_0^{-\frac{1}{8}}, & \text{initial motion downward,} \end{cases} \tag{5}$$

where x_0 is the distance between the ocean bottom disturbance and the base of the sloping beach measured in units of undisturbed water depth at the base of the sloping beach, and β is the beach slope.

6. Prediction of island run-up

Displayed in figure 9 are graphs of two-dimensional to one-dimensional linear amplification for various wavelengths and islands. Combination of these results with the one-dimensional solutions of Carrier allows a beach run-up prediction for a tsunami generated by a distant bottom disturbance, propagated over an irregular bottom, and amplified by an island slope.

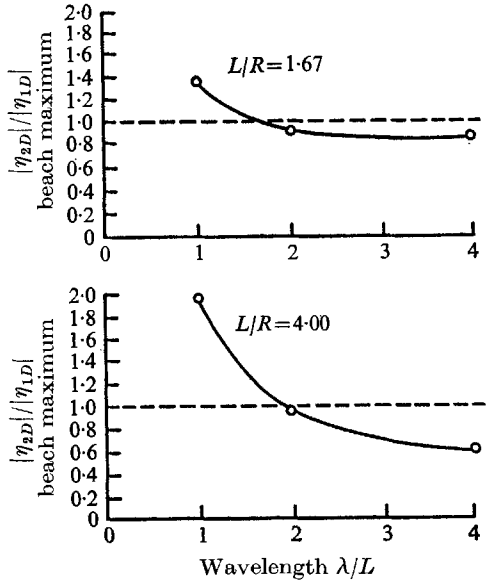

L/R	λ/L	$\lvert\eta_{1D}\rvert$	$\lvert\eta_{2D}\rvert$	$\lvert\eta_{2D}\rvert/\lvert\eta_{1D}\rvert$
1·67	1	4·02	5·48	1·36
	2	2·43	2·21	0·91
	4	2·10	1·79	0·85
4·00	1	5·16	10·03	1·94
	2	3·77	3·60	0·96
	4	2·38	1·54	0·65
4·65	0·785	6·59	11·50	1·73
	3·35	3·27	2·63	0·80
	7·85	2·10	1·10	0·52

$\bar{R}=|\eta|_{2-D}/|\eta|_{1-D}$, beach max.

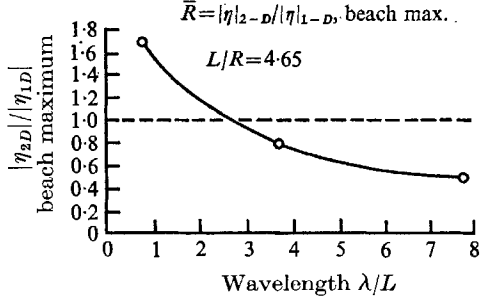

FIGURE 9. Ratio of two-dimensional to one-dimensional maximum wave amplitude on beach. L, island diameter at ocean floor; R, island diameter at beach.

A run-up estimate based on the full, nonlinear, two-dimensional long wave solution would be most desirable. A few observations obtained from analyzing the one-dimensional linear and nonlinear solutions make it possible to extrapolate known results into a prediction of island run-up. The solution on a sloping beach to the one-dimensional, nonlinear equations for small wave height, approaches exactly the linear solution over most of the sloping beach. Nonlinear effects are relegated to a small region adjacent to the beach, and essentially account for the details of a moving coast line, as waves advance and recede.

The region in which nonlinear terms are important for the one-dimensional case, i.e. the distance from shore where such effects are important, is small compared to the coastal radius of curvature of an island. Furthermore, in the shallow water, refraction implies that loci of constant phase are usually nearly parallel to the local coast line. Therefore, even in the two-dimensional case, nonlinear effects are approximately one-dimensional in nature. Also, the total run-up for the nonlinear case is equal to the total run-up predicted by the linear one-dimensional solution bounded at the quiescent coast line (Carrier & Greenspan 1958). The above remarks hold for a wave that does not break.

The beach amplification factor A (equation (5)) was obtained by a stationary phase calculation of integrals indicating that the maximum amplification is due to a small frequency band in the neighbourhood of the point of stationary phase. If a procedure analogous to that of Carrier in determining (5) could be followed for the two-dimensional, nonlinear solution, the expected result would again be an integral over frequency that could be evaluated by the method of stationary phase. The basic difference in the integrand would be a multiplicative term representing the three-dimensional geometrical effects.

Multiplicative separation of the final value would include two parts: a geometrical correction factor, and the amplification due to one-dimensional beach run-up. Since the maximum amplification is accounted for entirely by linear effects, a reasonable approximation to the geometrical correction factor is $\bar{R}$, the ratio of the maximum run-up of the single (stationary phase) frequency response on islands over the maximum run-up of the single (stationary phase) frequency response on straight beaches of identical slope; i.e.

$$\bar{R} = |\eta_{2D}|/|\eta_{1D}|.$$

Thus, the total amplification of a tsunami from island base to island coast is

$$A_{\text{total}} = \bar{R}.A. \tag{6}$$

$\bar{R}$ is given for the investigated islands in figure 9, and A, by (5).

7. Conclusions

Island run-ups will not always exceed run-ups of straight beaches. The wavelength involved must be sufficiently small with respect to the island diameter before refraction and diffraction overpower reflexion. In the cases studied, two-dimensional encroachment surpassed one-dimensional run-up for wavelengths less than twice the island base diameter.

The graphs of maximum wave amplitude *versus* angular position on the coast illustrate two other important features. The point of maximum inundation may occur to the side, as well as directly on the line, of reflective symmetry. For sufficiently small wavelengths, nodes and antinodes appear in the maximum amplitude curve. Consequently, one coastal section might experience relatively large amplitudes, while an adjacent area would be relatively unaffected.

The maximum amplitude around the coast may be associated with a 'circular wavelength' to identify the numbers of peaks and valleys for each incoming wavelength and island shape. Note that a 'circular wavelength' measured on an island circumference somewhere between the coast πR and the base πL is identical to the income wavelength.

As an example of the amplifications expected on the Hawaiian Islands, table 1 predicts the beach run-up for tsunamis initiated in the seismically active perimeter of the Pacific Ocean. The distances to various portions of the ocean circumference are such that the maximum run-up wavelengths do not differ significantly from the average wavelength of 100 nautical miles. The maximum beach amplification is determined by (5) and (6).

The amplification factors listed below are for round islands. Deviations from a circular coast found in nature may cause considerable change in maximum run-up. For example, the elliptical island run-ups (figures 5, 6) may be compared to the small island run-ups (figure 4). If Oahu is considered elliptic, the amplifications in the following table must be multiplied by 1·73 for a wavefront parallel to the major axis and 1·42 for a wavefront parallel to the minor axis.

	Maximum coastal amplification	
Island	Initial motion up	Initial motion down
Hawaii	6·39	8·52
Oahu (or Kauai)	12·37	16·50

TABLE 1

Though the preceding estimates are based on the assumption that the islands in the Hawaiian group are isolated, they are, in reality, reasonably adjacent. In fact, for the most part, the water between the islands is not as deep as the ocean floor. A more accurate picture would consider the islands as rising from an underwater ridge. The only island similar on all sides to the conical model is Kauai, but neighbouring Oahu still is sufficiently close to influence Kauai beach encroachment.

I am grateful to Professor George F. Carrier, whose counsel was of great significance in the successful execution of this project, and to Assistant Professor Donald G. M. Anderson for his most valuable guidance in the numerical work. This work was supported by the Office of Naval Research under Contracts Nonr-1866(20) and N000 14-67-A-0298-002, and by the Division of Engineering and Applied Physics, Harvard University.

Appendix A: derivation of the integral equation

Given (2) in vector notation,

$$h'\nabla^2\eta + \nabla h' . \nabla\eta + k^2\eta = 0, \tag{A 1}$$

where $$\nabla = \hat{\imath}\frac{\partial}{\partial x} + \hat{\jmath}\frac{\partial}{\partial z} \quad \text{and} \quad \nabla^2 = \frac{\partial^2}{\partial x^2} + \frac{\partial^2}{\partial z^2},$$

the following substitutions are made:

$$\eta(x,z) = e^{ik(x+\frac{1}{2})} + w(x,z) \quad \text{and} \quad h' = 1-h,$$

$$\nabla^2 w + k^2 w = -4\pi P(x,z) = h\nabla^2 w + \nabla h . \nabla w + ik(h\, e^{ik(x+\frac{1}{2})})_x. \tag{A 2}$$

Equation (A 2) is in the form of a non-homogeneous Helmholtz equation whose solution may be written in terms of an integral derived with the aid of Green's theorem and the appropriate Green's function.

The Green's function for the Helmholtz equation is derived formally from the equation,

$$\nabla^2 G(x,z,x',z') + k^2 G(x,z,x',z') = -4\pi\delta(x-x')\,\delta(z-z'), \tag{A 3}$$

where $\delta(x)$ is the Dirac delta function defined in the usual manner. The solution in an infinite region for outgoing waves is

$$G(x,z,x',z') = i\pi H_0^{(1)}(kR_1) \quad \text{where} \quad R_1 = ((x-x')^2+(z-z')^2)^{\frac{1}{2}},$$

and $H_0^{(1)}$ is the zero-order Hankel function.

Green's theorem states:

$$\oint_\Gamma (U\nabla V - V\nabla U).\hat{n}\,dl = \iint_A (U\nabla^2 V - V\nabla^2 U)\,dA. \tag{A 4}$$

The line integral path is the entire boundary of the surface integral domain and traversed such that the area under consideration lies to the left. $\hat{n}$ is the unit outward normal vector to the pathlength increment dl. w and G are substituted for U and V. A complete discussion of Green's functions and their applications is found in Morse & Feshbach (1953, pp. 791–895).

The case investigated includes a domain with water depth constant, save for an island centred on the origin. The area of the surface integral is the infinite, doubly connected region corresponding physically to the area occupied by the undisturbed water surface. The line integral in (A 4) consists of two pieces: the first, an integral around a closed contour at infinity; the second, an integral evaluated at the island coast.

The line integral evaluated around a closed contour approaching infinity, vanishes as a result of the limiting forms of w and G far from the island. w, in a constant depth domain, may be expressed in terms of a Hankel function expansion. The asymptotic forms of Hankel functions verify that

$$(w\nabla G - G\nabla w) \sim O(1/r^2),$$

as $r \to \infty$, where r is the distance from the island centre. Since the path length increases as r, the integral vanishes as $1/r$, $r \to \infty$. The normal procedure in problems of this nature is to require specific conditions on both w and G that will cause the line integral around the coast to vanish.

The only condition that w be bounded, makes it impossible to force the integral around the coast (Γ_1) to be zero. Alternatively, this integral is included as a term in the equation. Substituting for $\nabla^2 w$ and $\nabla^2 G$ by employing equations (A 2) and (A 3) results in the equation,

$$w = -\frac{1}{4\pi}\iint G(h\nabla'^2 w + \nabla' h.\nabla' w)\,dx'\,dz' - \frac{ik}{4\pi}\iint G(h\,e^{ik(x'+\frac{1}{2})})_{x'}\,dx'\,dz'$$
$$-\frac{1}{4\pi}\oint_{\Gamma_1}(w\nabla' G - G\nabla' w).\hat{n}dl'. \tag{A 5}$$

The contribution of the area integrals in (A 5) is everywhere zero except in the domain of the island. In its present form, (A 5) would require numerical integration of a numerically differentiated unknown, a process demanding a large number of grid points. Integration by parts removes the derivatives of the unknown from the integrals.

In vector form the first integral in (A 5) is

$$\iint_A G\nabla'.(h\nabla' w)\,dA' = \iint_A \nabla'.(Gh\nabla' w)\,dA' - \iint_A h\nabla' w.\nabla' G\,dA'. \quad \text{(A 6)}$$

Applying a version of Green's theorem

$$\left(\iint_A \nabla.\mathbf{B}\,dA = \oint_\Gamma \mathbf{B}.\hat{n}\,dl\right)$$

to the first integral on the right-hand side of (A 6),

$$\iint_A G\nabla'.(h\nabla' w)\,dA' = \oint_\Gamma Gh\nabla' w.\hat{n}\,dl' - \iint_A h\nabla' w.\nabla' G\,dA'. \quad \text{(A 7)}$$

The line integral consists of two parts, an integral around the island base circumference, and an integral around the island coast. The former vanishes ($h = 0$ at the island base), and the latter does not ($h = 1$ at the coast). Another integration by parts is performed on the second integral.

$$\iint_A h\nabla' w.\nabla' G\,dA' = \iint_A \nabla'.(wh\nabla' G)\,dA' - \iint_A w\nabla'.(h\nabla' G)\,dA'. \quad \text{(A 8)}$$

The first integral on the right-hand side is converted to line integrals as in (A 6) and (A 7), leaving the relation,

$$\iint_A G\nabla'.(h\nabla' w)\,dA' = \iint_A w\nabla'.(h\nabla' G)\,dA' + \oint_{\Gamma_1} h(G\nabla' w - w\nabla' G).\hat{n}\,dl'. \quad \text{(A 9)}$$

The substitution of (A 9) into (A 5) demonstrates that the line integrals in each equation cancel. The final form of (A 5) in polar co-ordinates (r, θ) is

$$\begin{cases} x' = r'\cos\theta', \\ z' = r'\sin\theta', \end{cases} \quad \begin{cases} x = r\cos\theta, \\ z = r\sin\theta, \end{cases}$$

$$wh' = -\frac{i}{4}\iint\left\{-k^2 H_0^{(1)}(kR_1)\,h + k\,\frac{H_1^{(1)}(kR_1)}{R_1}\,h_{r'}(r\cos(\theta-\theta') - r')\right\} wr'\,dr'\,d\theta'$$
$$+\frac{k}{4}\iint H_0^{(1)}(kR_1)\,e^{ik(r'\cos\theta + \frac{1}{2})}(\cos\theta' h_{r'} + ikh)\,r'\,dr'\,d\theta', \quad \text{(A 10)}$$

where $$R_1 = (r^2 + r'^2 - 2rr'\cos(\theta-\theta'))^{\frac{1}{2}}.$$

These results verify the validity of (A 10) (also (3)) in the infinite doubly connected domain in the neighbourhood of an island. Furthermore, (A 10) is valid in the singly connected domain in the neighbourhood of a seamount or submerged island (Lautenbacher 1967).

Two sets of elliptical co-ordinates were employed to handle elliptical islands with both major and minor axes perpendicular to the incoming wavefronts:

$$\begin{cases} x' = C_1\cosh\xi'\cos\phi', \\ z' = C_1\sinh\xi'\sin\phi', \end{cases} \quad \begin{cases} x = C_1\cosh\xi\cos\phi, \\ z = C_1\sinh\xi\sin\phi, \end{cases}$$

(major axis perpendicular to incoming wavefronts);

$$\begin{cases} x' = C_1\sinh\xi'\cos\phi', \\ z' = C_1\cosh\xi'\sin\phi', \end{cases} \quad \begin{cases} x = C_1\sinh\xi\cos\phi, \\ z = C_1\cosh\xi\sin\phi, \end{cases}$$

(minor axis perpendicular to incoming wavefronts).

Appendix B: numerical analysis

The working equation is a complex, singular, two-dimensional integral equation. The describing adjectives form an appropriate summary of the obstacles present. Complex variables were handled directly by the complex arithmetic module available on the IBM 7094 computer. The singularity of the equation

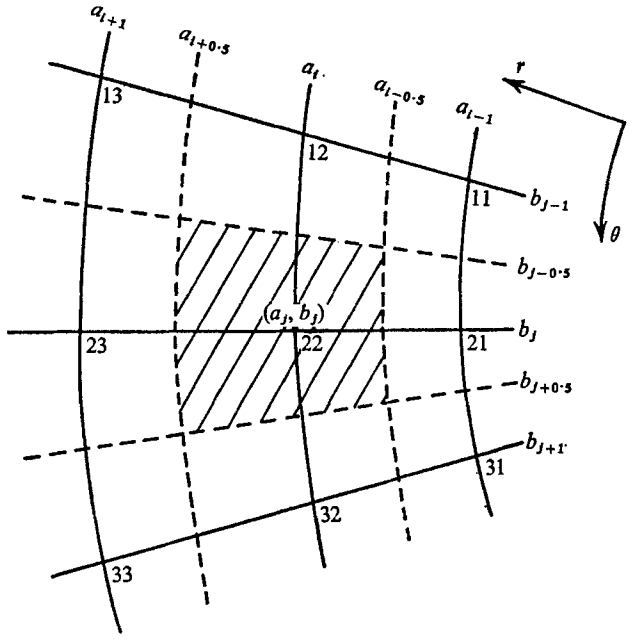

FIGURE 10. Circular mesh section. ——, mesh; – – – –, dual mesh.

required special treatment in the region of the singular point. With two dimensions involved, the numerical method had to be most efficient in the number of grid points necessary for an accurate solution. To determine the method of solution, the one-dimensional differential equation was solved analytically and compared with various numerical solutions of the one-dimensional integral formulation.

The successful approach included polynomial approximation of the unknown in the entire range of integration. The equation was written for each grid point, the integration performed, and the resulting set of linear, complex, algebraic equations solved by Gaussian elimination.

Specifically, the unknown $w(r, \theta)$ was approximated with bi-quadratics in r and θ using the Lagrangian interpolation polynomials:

$$l_1(r) = \frac{(r-a_2)(r-a_3)}{(a_1-a_2)(a_1-a_3)}, \qquad l_2(r) = \frac{(r-a_1)(r-a_3)}{(a_2-a_1)(a_2-a_3)},$$

$$l_3(r) = \frac{(r-a_1)(r-a_2)}{(a_3-a_1)(a_3-a_2)}, \quad w(r,\theta) = \sum_{i=1}^{3}\sum_{j=1}^{3} w_{ij}\, l_i(r)\, l_j(\theta);$$

$a_{1\cdot5} \leqslant r \leqslant a_{2\cdot5}$, $b_{1\cdot5} \leqslant \theta \leqslant b_{2\cdot5}$, w_{ij} are complex unknowns.

The range of integration was covered by assuming $w(r, \theta)$ to be a function composed of overlapping bi-quadratic segments connecting every three-point-by-three-point subdivision of the grid.

As an example (see figure 10), the crosshatched area was integrated assuming a biquadratic form for the unknown centred on point 22. The same technique was applied to every square of the dual mesh within the range of integration. Every term in the unknown equation matrix has contributions from integrations over nine blocks, each with its separate polynomial approximation. Every quadrature coefficient represents an average value of nine overlapping approximations.

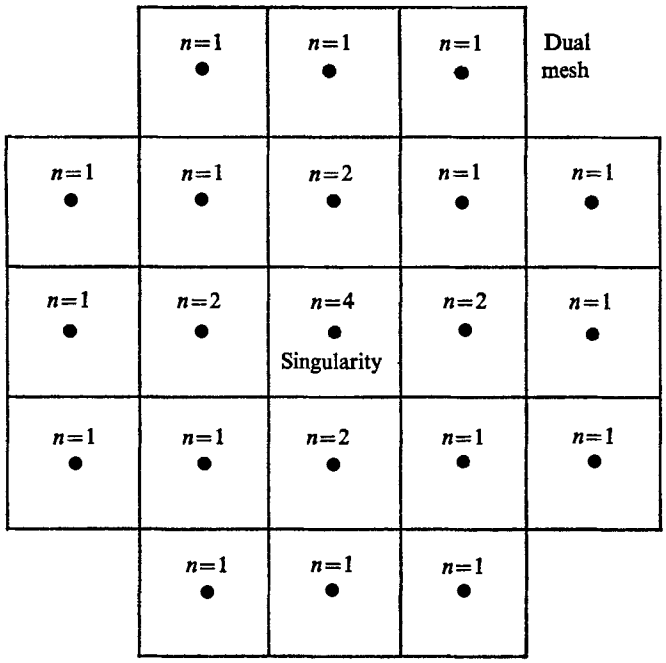

FIGURE 11. Singular integration scheme.

Hankel functions of order zero and one necessitated the numerical calculation of the quadrature coefficients. After testing various integration schemes, a product of two, three-point Gaussian quadrature formulae in r and θ was chosen. The integrals in schematic form are:

$$C_{mnij} = \int_{b_{j-0.5}}^{b_{j+0.5}} \int_{a_{i-0.5}}^{a_{i+0.5}} K(r_m, \theta_n, r', \theta')\, l_i(r')\, l_j(\theta')\, r'\, dr'\, d\theta',$$

where l_i are the Lagrangian interpolation polynomials defined above.

Sufficiently distant from the singularity at $r = r'$, and $\theta = \theta'$, the quadrature scheme was accurate to six significant digits (Lautenbacher 1967, p. A 22). Quadrature formulae compounded from the nine-point Gaussian quadrature were applied in dual mesh squares near to the singularity. Integral conversion was tested by gradually increasing the number of sample points and comparing the results. If n is the number of mesh spaces on each side of a dual mesh square, the

number of sample points is $9n^2$. So long as the singularity was not chosen as a sample point, integration in the singular regions presented no problem. For all parameter variations, the $n = 4$ results were correct to three significant figures (Lautenbacher 1967, p. A 24).

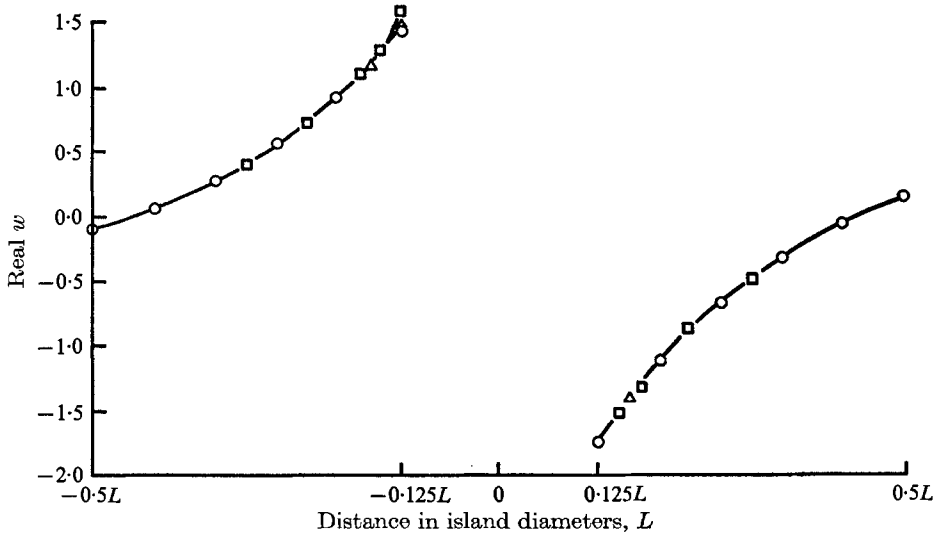

FIGURE 12. Convergence of two-dimensional solution on line of reflective symmetry ($\lambda = 2L$). ○, 42 points; ○ + △, 84 points; ○ + □, 130 points.

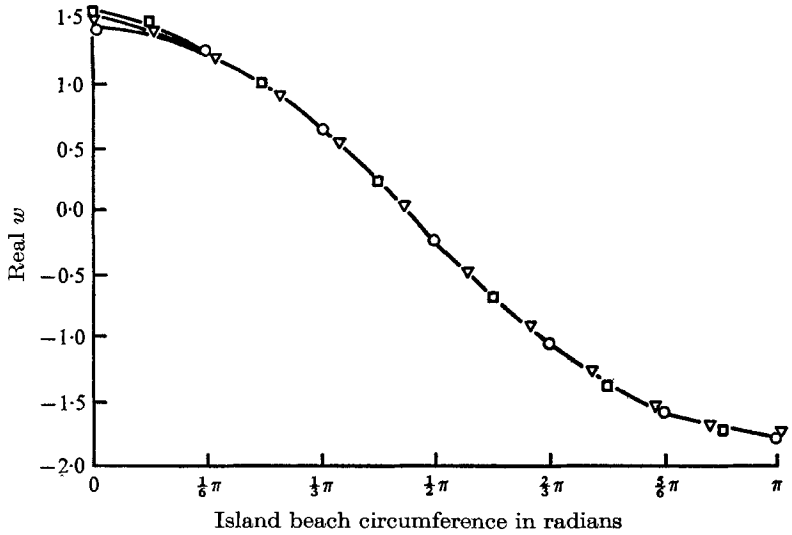

FIGURE 13. Convergence of two-dimensional solution around island at beach ($\lambda = 2L$). ○, 42 points; △, 84 points; ○ + □, 130 points.

As a check, integrals with simple $\ln R$ and $1/R$ singularities were computed both analytically and numerically. Results compared within 0·5 % when a sufficient number of sample points ($n = 4$) were used. The diagram in figure 11 indicates the number of sample points ($9n^2$) employed in the integration scheme

for all possible cases. The identical sampling procedure was employed for the nonhomogeneous term, a singular integral behaving like $\ln R$ as $R \to 0$.

By investigating islands with reflective symmetry, the number of unknowns was halved. Forty-two, eighty-four, and 130 unknowns on a half island were used. The running times on an IBM 7094 computer were 7, 20 and 60 min respectively. Solution convergence for an increasing number of grid points is shown in figures 12–13. Results for elliptical islands were computed by employing elliptical co-ordinates for the grids and the equations. The method was identical to the procedures outlined above.

REFERENCES

CARRIER, G. F. 1966 Gravity waves on water of variable depth. *J. Fluid Mech.* **24**, 641–659.

CARRIER, G. F. & GREENSPAN, H. P. 1958 Water waves of finite amplitude on a sloping beach. *J. Fluid Mech.* **4**, 97–109.

LAUTENBACHER, C. C. 1967 Gravity wave refraction by islands. Ph.D. Thesis, Harvard University.

MORSE, P. McC. & FESHBACH, H. 1953 *Methods of Theoretical Physics*. New York: McGraw-Hill.

VASTANO, A. C. & REID, R. O. 1966 A numerical study of the tsunami response at an island. *Texas A & M University Project* 471, *Reference* 66–26T.

VASTANO, A. C. & REID, R. O. 1967 Tsunami response for islands. *J. Marine Res.* **25**, 129–139.